ISSN: 1992-8645 www.jatit.org E-ISSN: 1817-3195

KIDNEY STONE DETECTION FROM DICOM IMAGES USING IMAGE PROCESSING TECHNIQUES

YUTI DEWITA ARIMBI[1], SARIFUDDIN MADENDA[2], LUSSIANA ETP[3]
[1]Gunadarma University, Department of Informatics, Jakarta, Indonesia
[2]Gunadarma University, Department of Information Technology, Jakarta, Indonesia
[3]Department of Information System [STMIK Jakarta STI&K]
E-mail: [1]yuti_dewita@staff.gunadarma.ac.id, [2]sarif@staff.gunadarma.ac.id, [3]lussiana@jak-stik.ac.id

ABSTRACT

Kidney stone detection from medical images is a critical step in early diagnosis and treatment planning. In this study, an image processing approach is proposed to identify kidney stones from DICOM (Digital Imaging and Communications in Medicine) files, focusing on both right and left kidney regions. The methodology includes grayscale conversion, elliptical area cropping, thresholding, and pixel counting to calculate kidney stone size. The results indicate significant differences in processing time and threshold values depending on the image characteristics. Based on the analysis, the shortest processing time was 1.30 seconds, while the longest reached 1.46 seconds, with an average of 1.32 seconds. It was also observed that images without kidney stones required approximately 1 second of processing time, while those containing kidney stones took between 20 to 40 seconds, depending on the size and number of stones. In one case (Sample 14), the processing time reached 2.21 seconds, reflecting the high pixel count (542 pixels) and larger stone area (322.59 mm²). The correlation analysis showed that the right kidney had a moderate positive relationship ($R = 0.57$, $R^2 = 0.33$), while the left kidney had a stronger correlation ($R = 0.94$, $R^2 = 0.88$), indicating more consistent pixel-to-area relationships. These findings demonstrate the effectiveness of the proposed image processing approach in identifying kidney stones with high accuracy, providing valuable insights for clinical decision-making and future improvements in automated kidney stone detection systems.

Keywords: *DICOM, Kidney Stone Detection, Image Processing, Pixel Analysis, Medical Imaging*

1. INTRODUCTION

The organs in the body that are in charge of regulating to control fluids in the body, especially for the urinary system, are the kidney organs. Another regulatory task by the kidneys is to control the level of salt in the blood, maintain a balance of acid and blood base levels, as well as problems with excretion of waste substances and excess salt levels [1]. When the kidney organs are reduced to the point where they are unable to filter the body's electrolyte removal, maintain the balance of body fluids and chemicals such as sodium and potassium in the blood or urine production, this is called kidney failure disease [2]. This results in the presence of a solid stone-shaped object caused by the deposition of various substances dissolved in urine in the urinary tract, known as kidney stones [3]. Kidney stones are formed from crystals that usually occur inside the kidneys which states that the crystals form inside the kidney tissue and take longer to develop into clinical stones [4].

Kidney stones cause patients to experience pain that requires emergency treatment and is one of the diseases whose prevalence continues to increase [5]. In the medical field, there is Randall's Plaque which is recognized as the origin of the formation of calcium oxalate stones. These plaques form on the surface of the renal papillae and become the initial site of crystal growth [6] and can lead to a risk of end-stage kidney failure [7]. Some of the main risk factors include hypercalciuria, a diet high in oxalate, and dehydration [8]. According to [9], genetic and environmental factors also play a role in the formation of kidney stones. Studies show that the heritability of nephrolithiasis is more than 45%. Accurate and prompt diagnosis is essential to determine the right treatment steps. Doctors generally diagnose kidney stone disease using various imaging techniques, one of which is a manual interpretation-based method with medical imaging. However, it takes a long time and relies on the experience of radiologists to get information on whether the patient has kidney stone disease.

Therefore, it is necessary to develop an artificial intelligence-based system to help the process of detecting kidney stones more efficiently with CT scan images being the most commonly used method to provide a clear and detailed picture of the internal structure of the kidneys and urinary tract [10]. Image-processing-based renal stone detection methods can accurately classify and report the presence of stones in the kidneys, potentially improving early detection and treatment [11].

Various imaging and image analysis techniques have been developed to improve the accuracy and efficiency in detecting kidney stones. One example is the accuracy of detection of kidney stones with more detailed texture analysis in predicting the success of medical procedures and reducing the need for manual measurements [12]. A framework features optimized combined texture designed to identify kidney stones. These combined texture features include GLCM, RLM, and Histogram. The optimized feature data is then used for four machine vision classifiers, namely Random Forest, MLP, j48, and Naïve Bayes. The best results are obtained with Random Forest with 90% accuracy at 22x22 ROI [13]. Segmentation of kidney stones in medical ultrasound images is a difficult task due to variations in object shape, orientation, and image quality. The method proposed in this study uses contour transformation and contrast enhancement using histogram equalization for renal ultrasound image preprocessing [14]. Other studies, such as graphical representations of numerical data distributions, can be used to analyze the texture and intensity of medical images.

In detecting kidney stones, histograms can be used to measure the density of kidney stones and predict the success of medical procedures such as retrograde intrarenal surgery (RIRS) [15]. In his study, histograms from Hounsfield units (HU) on non-contrast CT scans could be used to predict the success of "stone dusting" during RIRS. Successfully dusted stones have a wider HU range and higher standard deviations. Meanwhile, the HU volume that is most often measured is smaller in the stone that has been successfully dusted. Evaluation of the HU histogram showed differences in distribution and proportion, which helped predict surgical outcomes and prepare for intraoperative complications [15].

Prediction of a fragility in kidney stones using histograms as an attenuation value of kidney stones measured using helical CT without contrast. Parameters such as TSV, mean attenuation value (MAV), and peak presence (HE) on the histogram were compared between the successful and failed treatment groups. Research indicates that HE values are found to be independent predictors of the success or failure of extracorporeal shock wave lithotripsy (ESWL) [16]. Another study developed an automatic stone detection system from CT images using a Support Vector Machine (SVM). Where before classification, images were improved such as histogram equalization and emboss. The results of the study achieved an accuracy of 98.71% by testing 156 CT samples that had kidney stones or tumors as well as healthy kidneys [17].

In improving image quality and better segmentation through histogram equalization techniques in ultrasound imaging, the histogram equalization approach is used to reduce noise and improve contrast. This technique aids in optimal segmentation and detection of kidney areas [18]. Another thing in the utilization of the Gaussian filtering method and Contrast Limited Adaptive Histogram Equalization (CLAHE) is applied to improve image quality before segmentation is carried out based on image entropy [19], [20].

While several automated systems have been proposed for nephrolithiasis detection, a significant challenge remains in the computational efficiency versus accuracy trade-off. Recent studies in 2024 [21], and [22] have utilized complex deep learning architectures that achieve high accuracy (>95%) but require substantial computational resources and lack transparency in feature extraction. There is a critical 'grey area' in current literature regarding the optimization of threshold-based segmentation for DICOM metadata without relying on heavy neural networks, which often fail resource-constrained clinical settings.

This research aims to develop a semi-automated system that utilizes CT scan images to detect kidney stones with high accuracy. One of the methods used that can help identify and classify kidney stones is histogram analysis based on image characteristics. However, there is low noise and contrast in ultrasound images (CT scans) which can affect the accuracy of detection. Based on these constraints, the purpose of the study is to utilize the histogram of an image from a CT scan of kidney stones in handling noise and optimization of features can still be overcome to achieve optimal results in detecting kidney stones.

2. RESEARCH METHODOLOGY

This study aims to develop a system for detecting kidney stones based on CT scan images in DICOM format, as well as obtaining information on the area

ISSN: 1992-8645 www.jatit.org E-ISSN: 1817-3195

area by utilizing the number of pixels from each kidney stone found. In Figure 1, a research flow diagram is shown that explains the system process in a comprehensive manner.

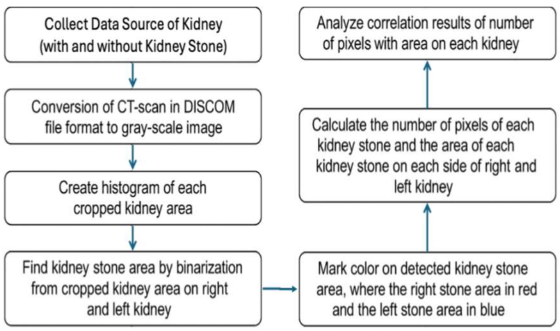

Figure 1: Our proposed methodology for diagnosing kidney stones leverages image processing techniques applied to CT scan data.

2.1 Data Source of the CT-Scan

The image data collected was secondary data with the diagnosis of kidney stones as many as 13 images and 4 images with the diagnosis result of not finding kidney stones in the kidney area. The image data in this study came from the Radiology Department of Cipto Mangunkusumo Hospital (RSCM) which was taken from the hospital's patients consisting of children to adults. Image data was obtained from the Computed Tomography (CT) Scan tool. CT is a well-established and widely used tissue imaging technique in the medical world for non-invasive clinical diagnostics that allows for 3D visual reconstruction and segmentation of tissues of interest.

High-resolution CT systems can be used to perform non-destructive 3D imaging of various types of tissues and organ systems, such as the gastrointestinal tract, cardiovascular system, renal tract, liver, lungs, bones, cartilage, tumor tissues, and more [23]. However, CT also has some drawbacks such as fairly high radiation exposure, image artifacts, and side effects of the contrast medium provided [23]. CT is based on the attenuation of X-rays passing through the object being examined. The linear X-ray attenuation coefficient is calculated separately for each voxel, i.e. cuboid volumetric elements make up each scanned layer, and converted to Hounsfield units (HU) to estimate density and are arranged in the form of the Hounsfield scale [24]. CT imaging is performed by rotating an X-ray source around an object, with the detector positioned directly opposite the radiation source. The resulting projections are then mathematically processed to create a 3D rendition of the scanned object [25]. The thickness of the slice in the image is 5 mm, and the pixel size is 512x512 pixels, the pixel spacing size of the DICOM image in millimeters (mm) has different values. CT scan images are stored in Digital Imaging and Communication in Medicine (DICOM) format with the extension *.dcm. CT scan image is an image of the results of CT scan images in detecting kidney stones shown in figure 2a .

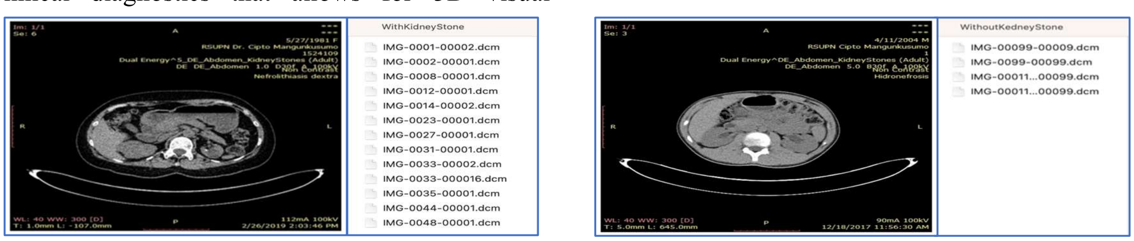

(a) (b)

Figure 2: Images of a patient with a diagnosis (a) with a kidney stone, (b) without a kidney stone

2.2 Convert Grayscale Image Format

The research process began by converting CT-Scan data in DICOM (Digital Imaging and Communications in Medicine) format to grayscale image format. DICOM is a standard format for storing medical images, including CT-Scan data, which contains image information as well as metadata such as resolution, slice thickness, and pixel spacing. This conversion is important because DICOM data typically has multiple layers of information that need to be simplified into grayscale imagery for further analysis. Grayscale image conversion is essential as it ensures that each pixel contains a single intensity value, simplifying the segmentation and area measurement of kidney stones. Pseudo-code for this step:

Algorithm 1: DICOM to Grayscale Image Conversion

Input: DICOM file (e.g., CT-Scan data)
Output: Grayscale image

1. Load DICOM file
2. Extract DICOM image data
3. Get image resolution (Rows x Columns)
4. Calculate pixel dimensions
5. Convert to grayscale
6. Display the grayscale image

The first step is to load the DICOM file, which contains the CT-Scan image and essential metadata such as pixel spacing, resolution, and patient information. DICOM (Digital Imaging and Communications in Medicine) is the standard format used for medical images, ensuring that each pixel in the image can be accurately related to real-world measurements. This step is critical, as it provides the foundational data needed to calculate the physical area of detected kidney stones. Without this information, the subsequent steps of image processing and analysis would lack the spatial context required for accurate measurements.

The second step involves extracting the raw image data from the DICOM file using the *DICOM Read* function. This function retrieves the pixel values from the CT-Scan, which are essential for image processing. In some cases, a color map (MAP) is also returned, which is typically used for indexed color images. However, for medical CT scans, this color map is often ignored because the image is already in grayscale or needs to be converted to grayscale for further analysis. This step ensures that only the relevant pixel intensity information is processed, reducing the complexity of subsequent analysis steps. The third step is to retrieve the image resolution, which is defined by the number of rows and columns in the DICOM file. This information is critical for determining the total number of pixels available for analysis. It provides the basic spatial context needed to calculate the physical size of the kidney stone, as the total pixel count directly impacts the measured area. Without accurate resolution data, the calculated stone area could be significantly overestimated or underestimated, leading to incorrect clinical assessments.

Next step (Calculate Pixel Dimensions) involves calculating the physical area of each pixel based on the pixel spacing information obtained from the DICOM metadata. The pixel spacing is usually provided in millimeters and represents the real-world size of each pixel in both the horizontal (x) and vertical (y) directions. By multiplying these two values, the area of each pixel can be determined in square millimeters (mm^2). This conversion is essential because it allows the total pixel count, obtained during the segmentation process, to be accurately translated into the physical area of the kidney stone, providing a realistic estimate of stone size. In the next step (Convert to Grayscale), the raw image data is normalized and converted into a standardized grayscale format where pixel intensities range between 0 and 255.

This normalization process ensures that variations in image brightness and contrast are minimized, allowing consistent and reliable analysis in the subsequent image processing stages. In the final step, the converted grayscale image is visually presented to the user. This allows for manual verification that the conversion process has accurately transformed the DICOM data into a clear and analyzable grayscale image, setting the stage for precise subsequent image processing steps.

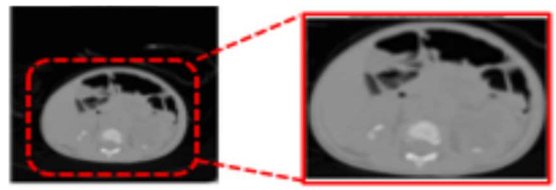

Figure 3: The grayscale image original and after Crop

After converting the CT-Scan image to grayscale, the main area containing the kidney structures is cropped, as illustrated in Figure 3. The cropping process isolates the kidney regions, it can be observed that the right and left kidney areas have different dimensions, reflecting the natural anatomical variations in kidney shape and size. The primary purpose of this cropping process is to clearly isolate the right and left kidney regions. This step is crucial for reducing background noise and avoiding interference from surrounding tissues, which can significantly impact the accuracy of kidney stone detection. By focusing only on the relevant kidney areas, the subsequent image processing and analysis can be performed with higher precision, ensuring that measurements such as stone size, shape, and distribution reflect the actual clinical condition.

2.3 Histogram the Right and Left Kidney Areas

The next step is to extract the right and left kidney areas separately. This is done to ensure that the analysis focuses on each kidney independently. The kidney area is cropped by defining boundary coordinates or using segmentation algorithms to detect kidney contours. This technique helps avoid interference from surrounding tissues that could disrupt the measurement of kidney stones. This separation is also crucial for the final correlation analysis, where the characteristics of the right and left kidney stones can be compared independently. This process is done by asking the user to interactively select the coordinates that define each of the areas shown in algorithm 2.

Algorithm 2: Manual Region Selecting and Cropping of the Kidney Area from Grayscale Image

Input: Grayscale kidney image
Output: Two separate cropped regions (right and left kidney areas)

Journal of Theoretical and Applied Information Technology
31st March 2026. Vol.104. No.6
ISSN: 1992-8645 www.jatit.org E-ISSN: 1817-3195

1. Load Grayscale Image
2. Select First Region (Right Kidney)
3. Select Second Region (Left Kidney)

The explanation of the steps in algorithm 2 is as follows; (1). Read and Prepare The image to be processed is a grayscale image that has been pre-cropped, stored in a certain variable (e.g. variable t). (2). Select the First Area (Right Kidney) by determining the top-left and bottom-right boundaries of the area to be cut. These coordinates are used to extract the corresponding parts of the image. The results are stored in variable a. (3). Do the same for the selection of the Second Area on the left kidney, the result is stored in variable b.

The kidney areas selected; intensity histograms are generated for each region to analyze pixel distribution. These histograms represent the frequency of pixel intensities within each kidney area, which can help determine appropriate threshold values for the binarization process in the following step. Histogram analysis is also useful for identifying the intensity range most likely to correspond to kidney stones, which typically have higher intensity values compared to normal kidney tissue.

Algorithm 3: Histogram Generation for Kidney Areas

Input: Cropped right kidney image (example: a), and cropped left kidney image (example: b)
Output: Histograms Graphics for each kidney area

1. Generate histogram for right and left kidney area
2. Find the threshold value
3. Display the histograms and Threshold value

This algorithm creates histograms for each cropped kidney area to visualize the distribution of pixel intensities, which is essential for accurate kidney stone detection in subsequent processing steps. The graphics of histogram can be seen in figure 4.

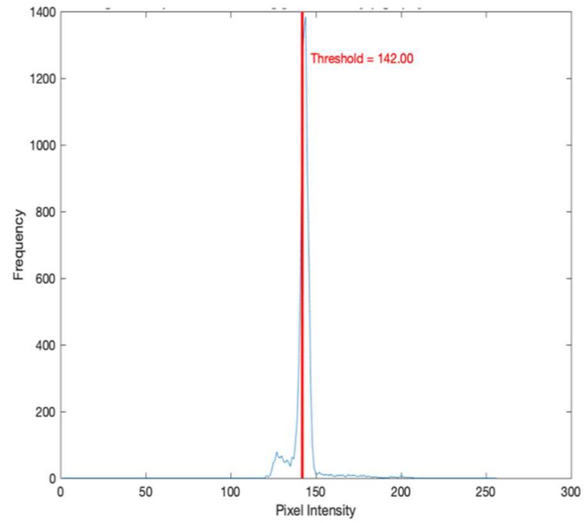

Figure 4: Histogram with Threshold

2.4 Finding the Kidney Stone (In the Side Right and Left Kidney) Areas

Based on the dynamically obtained thresholds from the histogram analysis of each kidney area, the detection of kidney stones can be performed more accurately and automatically. This approach utilizes the histogram to assess the pixel intensity distribution within each cropped kidney region, both for the right and left kidneys. By determining an appropriate threshold, regions with higher intensity values, which are most likely to represent kidney stones, can be effectively separated from normal tissue.

This threshold plays a critical role in the image binarization process, where pixels with intensity values above the threshold are classified as kidney stones, while those below are considered soft tissue. As a result, the visual output for each kidney area clearly indicates whether kidney stones are present or absent. The right and left kidney stones can be detected independently, enabling more accurate analysis, especially when the size or distribution of the stones differs between the two sides.

Algorithm 4 allows the user to manually select for the right kidney and left kidney areas by pinning two points on the image using the ginput() function in MATLAB. For example, the selection of the right ginal area for the first point (x11, y11) is used as the upper left corner, and the second point (x12, y12) is the lower right corner of the area to be cut. Once the point is selected, these coordinates are converted to integers to ensure a valid matrix index. Then, the image area between these two points is extracted to produce a cropped image (a), while a crop image for the left kidney is placed on (b). Both crop image results will be displayed for result verification.

Algorithm 4: Image Cropping with Manual Point Selection

Input: Image (t) are original image
Output: Image (a) are cropped image based on user-selected the right kidney areas, and image (b) are cropped image based on user-selected the left kidney areas,

1. Select the first corner (top-left) of the cropping area to get the first coordinate (x11, y11)
2. The second corner (bottom-right) of the cropping area to get the second coordinate (x12, y12)
3. Crop the selected area (right kidney area) from the original image (t), which extract the region from (x11, y11) to (x12, y12) and create image (a) as new figure
4. Loop step 1 until step 3 for left kidney area, which the first coordinate (x21, y21) and the second coordinate (x22, y22) and create image (b) as new figure
5. Display the cropped image output: the right kidney area saving to variable (a) and the left kidney area saving to variable (b)

In algorithm 4, kidney stone may be found or not, but this approach also allows for the identification of kidney stones of varying sizes and shapes, without the need for manual adjustments for each image, thus speeding up the diagnostic process and improving the accuracy of detection in medical image processing systems. Furthermore, this method can be combined with advanced segmentation algorithms to enhance detection sensitivity, making it a more reliable solution for clinical applications. A visualization of the results of both selected areas can be displayed to ensure that the area is cut correctly (see Figure 5).

(a) Right Kidney Area (b) Left Kidney Area

Figure 5: Image crop.

The primary stage in obtaining images that identify the presence of kidney stones involves the binarization process. After isolating the kidney areas as shown in Figure 5, the next step is to compare the intensity values of each pixel within these regions against a predetermined threshold. In this process, any pixel with an intensity value greater than the threshold is converted to white, indicating a potential kidney stone, while pixels with values below the threshold are converted to black, representing the surrounding soft tissue.

Algorithm 5: Manual Region Selecting and Cropping of the Kidney Area from Grayscale Image

Input: Image cropped regions (right/left kidney areas)
Output: Binary Image (right and left kidney areas)

1. Initialize a blank Binary Image with the same dimensions as the image of the right (a) and left (b) kidneys.
2. Binary Process for the Right Kidney:
   - ✓ Loop through each pixel in a picture.
   - ✓ If the pixel intensity value is greater than the threshold value, it is considered a kidney stone and is given a value of 255 (white).
   - ✓ Otherwise, the pixel is rated 0 (black).
3. Binary Process for Left Kidney (Same process applied in figure b)
4. Binary image output (right kidney and left kidney)

The algorithm 5 effectively highlights the regions of interest, as illustrated in Figure 6, providing a clear distinction between kidney stones and normal kidney structures.

(a) Right Kidney Area (b) Left Kidney Area

Figure 6: Binary Image Conversion.

2.5 Output the image for Kidney Stone Areas

The process of outputting the Image for kidney stone areas is an important step in visualizing the results of kidney stone detection. The results of the image processing for kidney stone detection are visually presented with clear annotations to distinguish between stones identified in the right and left kidney regions. After the binarization process, each kidney area is analyzed separately to accurately identify the presence of stones. To enhance the interpretability of the results, color markings are applied to highlight the detected kidney stones. Specifically, stones in the right kidney are marked in red, while those in the left kidney are marked in blue, as illustrated in the annotated output images.

This color-coding approach helps clinicians quickly differentiate between stones in each kidney, reducing the risk of diagnostic errors and improving the overall efficiency of the analysis. In addition to visual markings, a legend is included in each output image to provide a clear reference for interpreting the color codes. This combination of visual and textual information ensures that the analysis results are both comprehensive and easy to interpret, supporting accurate clinical assessments.

Journal of Theoretical and Applied Information Technology
31st March 2026. Vol.104. No.6
© Little Lion Scientific

ISSN: 1992-8645 www.jatit.org E-ISSN: 1817-3195

Furthermore, the use of separate color codes for each side also facilitates the comparison of stone size, distribution, and density, which can be critical for determining the appropriate treatment plan. The algorithm 6 are approach significantly improves the clarity and precision of the diagnostic output, making it a valuable tool for automated kidney stone detection systems.

Algorithm 6: Kidney Stone Marking with Color Legends

Input: Binary images in right kidney and left kidney
Output: Image with kidney stones marked in different colors for right and left sides

1. Initialize the coordinates and dimensions of the cropped regions: (x1, y1) for the right kidney area and (x11, y11) for the left kidney area
2. Loop through each pixel in the right kidney region:
   - For n_i = 1 to length the Rows:
     - For m_i = 1 to length the Columns:
       - If the pixel value at (x_i, y_i) in right kidney is 255 (stone detected):
         - Plot the pixel at (x1 + y_i - 1, y1 + x_i - 1) in red with size 1
3. Loop through each pixel in the left kidney region:
   - For n_{ii} = 1 to length the Rows:
     - For m_{ii} = 1 to length the Columns:
       - If the pixel value at (x_{ii}, y_{ii}) in left kidney is 255 (stone detected):
         - Plot the pixel at (x11 + y_{ii} - 1, y11 + x_{ii} - 1) in blue with size 1
4. Add legends to the image (a red the legend for the right kidney stone, and a blue the legend for the left kidney stone). If the image original has not the legend, that image are not found kidney stone.
5. Display the final annotated image

Algorithm 6 aims to provide visual marks on the areas detected as kidney stones on the right and left sides of the kidney, making it easier for medical personnel to interpret the results. In Algorithm 6, each pixel identified as a kidney stone is colored marked to distinguish the location and side of the kidney. Kidney stones on the right kidney are marked in red, while kidney stones on the left kidney are marked in blue. This approach ensures that both areas of the kidney can be analyzed separately, while reducing the risk of errors in the calculation of the number and area of kidney stones. This algorithm works by examining each pixel in the segmented binary image ($image_a$ for the right kidney and $image_b$ for the left kidney). If the pixel has an intensity value of 255 (white), it is considered a kidney stone and is marked with a color mark according to the side of the kidney. The results of this visualization are then displayed as a final image, as shown in Figure 7, where each detected kidney stone is colored for further identification and analysis.

The application of different colors to each side of the kidney also helps in comparative analysis, such as comparing the number, size, and distribution of kidney stones between the right and left kidneys, which is important for more precise treatment planning.

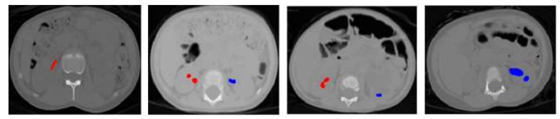

(a) Result with kidney stones (red: kidney stone in the right, blue: kidney stone in the left)

(b) Result without kidney stones

Figure 7: The result of detection kidney stone

2.6 Calculating the Number of Pixels and Area of Each Kidney Stone

After the segmentation and binarization processes to extract kidney stone areas from CT-Scan images, the next critical step is to calculate the number of pixels and the area of each detected stone. This measurement is essential for determining the size and severity of kidney stones, which are key clinical parameters in selecting appropriate treatment strategies.

Algorithm 7: Pixel Count for Kidney Stone

Input: Binary image of kidney stone (binaryImage)
Output: Total pixel count

1. Load the binary image (binaryImage = segmented kidney stone image)
2. Initialize the pixel counter (example X = 0)
3. Loop through each pixel in the binary image
   - For i = 1 to Rows:
     - For j = 1 to Columns:
       - If binaryImage(i,j) == 255:
         - Increment pixel counter
4. Return the total pixel count

In algorithm 7, the process begins by identifying each connected group of pixels (connected components) in the binary image. Each connected group is considered a single kidney stone if it meets certain criteria, such as minimum size and shape requirements. Once each stone is identified, the total number of pixels within each group is counted. Convert the pixel count into a physical area measurement (mm²), the pixel spacing information from the DICOM file metadata is used. This metadata provides the real-world width and height of each pixel in millimeters. Using the following equation:

$$\text{Area}_{\text{Kidney Stone}} = \sum_{i=1}^{n} Pixel_i \times Area_j \quad (1)$$

Where $\text{Area}_{\text{Kidney Stone}}$ is the total area of the kidney stone in square millimeters (mm²), $\sum_{i=1}^{n} Pixel_i$ is the total pixel count, and $Area_j$ is the physical area of each pixel, typically obtained from the Pixel Spacing metadata in the DICOM file.

This approach provides a more objective estimate of kidney stone size compared to manual measurement methods, reducing potential errors in interpretation. After the area is calculated, these results can be used to compare the size of stones between the right and left kidneys, as well as to monitor the growth or reduction of stones over time. The information is crucial for planning medical procedures such as lithotripsy or surgical stone removal. In our researcher, the result of the information is shown in figure 8.

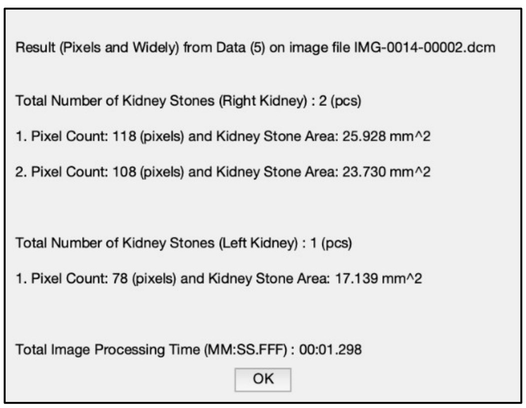

Figure 8: The result of information about kidney stone

Figure 8 illustrates the results of image processing used to diagnose the presence of kidney stones on the right and left sides of the kidneys. In this experiment, the researcher used image data 5, which underwent a series of image processing steps, including grayscale conversion, segmentation, binarization, and color marking for each detected kidney stone.

The processing time measurement is conducted after the binary image conversion, as the initial steps involve ellipse-shaped area cropping and segmentation to isolate the right and left kidney regions. These preliminary processes are essential to reduce the image area, focusing only on the kidney regions for more accurate stone detection. From this image analysis, it was found that the right kidney contains 2 kidney stones, while the left kidney has 1 kidney stone. Each detected kidney stone is marked with different colors to distinguish the sides, with red for the right kidney and blue for the left kidney. n the experiment using image data 5, the total processing time required for this data set was 1.298 seconds. This includes all steps from area segmentation, thresholding, binarization, and stone marking, reflecting the efficiency of the implemented image processing algorithm.

In addition to the number of kidney stones, this analysis also includes the calculation of pixel count and area for each kidney stone, which are determined based on the total number of pixels forming each stone and converted into square millimeters (mm²) using the Pixel Spacing information from the DICOM file metadata. This information is crucial for determining the physical size of the kidney stones, which significantly influences the choice of treatment methods.

In Figure 8, the right kidney has a total of 2 stones, with the following details:

- The first kidney stone has 118 pixels with an area of 25.928 mm²
- The second kidney stone have 108 pixels with an area of 23.730 mm²

Meanwhile, the left kidney has 1 stone with the following details:

- The third kidney stone have 78 pixels with an area of 17.139 mm²

This information provides a clearer overview of the distribution, size, and number of kidney stones on both sides, aiding in more accurate medical decision-making.

2.7 Analysis of the Correlation between the Number of Pixels and the Area of the Kidney Stones

The methodology of correlation analysis between the number of pixels and the area of kidney stones aims to evaluate the linear relationship between the digital size of kidney stones in the form of pixels and their size in physical units (mm²). This analysis is important to ensure that the results of the detection of kidney stones from medical images have accuracy consistent with the actual size, which is necessary for diagnosis and clinical decision-making (see algorithm 6). After the $\sum_{i=1}^{n} Pixel_i$ and $\text{Area}_{\text{Kidney Stone}}$ obtained for each kidney stone, correlation analysis was performed to evaluate the relationship between these two variables. This correlation is calculated using the Pearson correlation coefficient (R), which measures the strength and direction of the linear relationship between the number of pixels and the area. The value of R ranges from -1 to 1, where a value close to 1 indicates a very strong and positive relationship, while a value close to 0 indicates a weak relationship or no relationship.

Algorithm 8: Correlation Analysis with Linear Regression

Input:
- Variable X = $\sum_{i=1}^{n} Pixel_i$ are array of pixel counts for each kidney stone
- Variable Y = $\text{Area}_{\text{Kidney Stone}}$ are array of corresponding kidney stone areas (mm²)

Output:
- R: Correlation coefficient (Pearson)
- R^2: Coefficient of determination
- Regression Line: Slope and intercept for linear model

1. Initialize the data using the pixel count array (X) and the area array (Y)
2. Calculate the Pearson correlation coefficient (R):
   - Compute the covariance between X and Y
   - Divide by the product of the standard deviations of X and Y
3. Perform linear regression to find the best fit line by calculate the slope (m) and intercept (b) using:
   - **m = covariance (X, Y) / variance(X)**
   - **b = mean(Y) - m * mean(X)**
4. Calculate the coefficient of determination (R^2):
   - **R^2 = (covariance (X, Y) / (std(X) * std(Y)))^2**
5. Display plot the data and regression line:
   - Create a scatter plot of X and Y
   - Plot the regression line using the equation **Y = m * X + b**
   - Add titles, labels, and legends
6. Output the correlation coefficient (R) and R^2

3. RESULTS AND DISCUSSION

The results of this study provide significant contributions to the field of healthcare, particularly in the diagnostic process using CT-Scan images, as illustrated in Figure 9. This approach enables the automated detection of kidney stones through advanced medical image processing techniques. Based on the set of image data that have been converted to grayscale, all images have a standard dimension of 512x512 pixels, which is a typical resolution for CT-Scan images.

These differences in kidney area dimensions are due to the physiological variations between the right and left kidneys, as well as their position and orientation, which can vary from patient to patient. The specific dimensions of the right and left kidney areas after cropping are presented in Table 1, highlighting the variability in area size for each processed image.

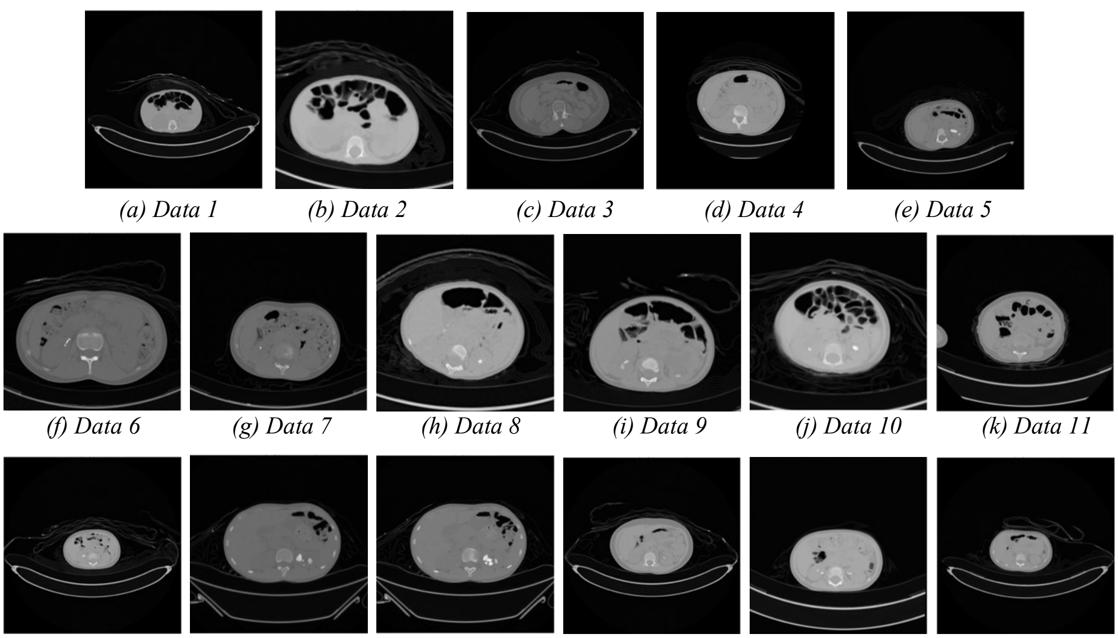

(a) Data 1 (b) Data 2 (c) Data 3 (d) Data 4 (e) Data 5
(f) Data 6 (g) Data 7 (h) Data 8 (i) Data 9 (j) Data 10 (k) Data 11
(l) Data 12 (m) Data 13 (n) Data 14 (o) Data 15 (p) Data 16 (q) Data 17

Figure 9: The original image after converting gray scale.

Journal of Theoretical and Applied Information Technology
31st March 2026. Vol.104. No.6

ISSN: 1992-8645 www.jatit.org E-ISSN: 1817-3195

Table 1: The variability in area size, number of kidney stones, time processing, threshold, and code data sample.

Number	File Name (file format DICOM with extension *.dcm)	Code Data Sample	Number of Kidney Stone		Resolution Size (pixels)		Threshold (Pixel Intensity)	Processing Time (Seconds)
			Right Area	Left Area	Image Original	ellipse-shaped area		
1	IMG-000111-000099	Data 1	0	0	512 x 512	182 x 130	141	1.03
2	IMG-0001111-000099	Data 2	0	0	512 x 512	373 x 266	177	1.08
3	IMG-00099-00009	Data 3	0	0	512 x 512	296 x 195	101	1.07
4	IMG-0099-00099	Data 4	0	0	512 x 512	259 x 198	146	1.02
5	IMG-0001-00002	Data 5	0	2	512 x 512	209 × 156	125	1.33
6	IMG-0002-00001	Data 6	1	0	512 x 512	442 × 281	104	1.35
7	IMG-0008-00001	Data 7	2	0	512 x 512	323 x 235	109	1.33
8	IMG-0012-00001	Data 8	0	1	512 x 512	364 x 296	163	1.17
9	IMG-0014-00002	Data 9	2	1	512 x 512	370 x 286	142	1.30
10	IMG-0023-00001	Data 10	1	1	512 x 512	342 × 281	175	1.46
11	IMG-0027-00001	Data 11	2	0	512 x 512	263 × 216	144	1.31
12	IMG-0031-00001	Data 12	3	0	512 x 512	172 x 124	155	1.26
13	IMG-0033-000016	Data 13	0	4	512 x 512	343 × 244	106	1.67
14	IMG-0033-00002	Data 14	0	2	512 x 512	343 × 238	120	2.21
15	IMG-0035-00001	Data 15	0	3	512 x 512	246 x 170	149	1.33
16	IMG-0044-00001	Data 16	2	1	512 x 512	275 × 186	167	1.32
17	IMG-0048-00001	Data 17	1	1	512 x 512	188 × 130	148	1.20

3.1 Threshold (Pixel Intensity)

Based on Table 1, the histogram analysis results show the pixel intensity range in the sample image data used in this study. From the table, it can be observed that the lowest pixel intensity is 101 (code data sample is data 3), while the highest pixel intensity reaches 177 (code data sample is data 2). This range reflects the variation in tissue density within the kidney region, which is critical for the accurate detection of kidney stones. The threshold value obtained from the histogram analysis serves as a dynamic reference for identifying kidney stone areas more precisely. Using this threshold, each pixel in the image with an intensity value higher than the threshold is classified as a kidney stone, while pixels with lower intensity values are considered as soft tissue.

The pixel intensity results from each image produce different threshold values, where sample data 13 and sample data 14 represent CT-Scan results from the same patient diagnosed with kidney stones. However, these two images have different threshold values; sample data 13 has a threshold of 106, while sample data 14 has a higher threshold of 120. That difference in threshold values results in variations in the number of detected kidney stones. In the left kidney area of sample data 13, 4 pieces of kidney stones were identified, whereas sample data 14 only contains 2 pieces of kidney stones. This discrepancy is primarily due to the lower overall pixel intensity in sample data 13 compared to sample data 14.

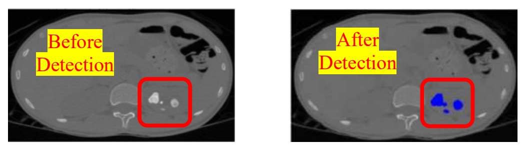

(a) Data sample 13 (Threshold = 106)

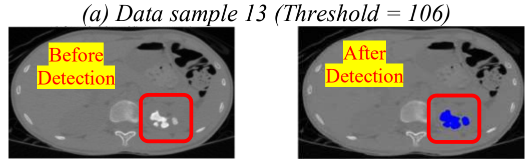

(b) Data sample 14 (Threshold = 120)

Figure 10: The experiment of the same patient diagnosed

The test results for these two images can be seen in Figure 10, which clearly illustrates how the variation in threshold values impacts the detection of kidney stones. This approach allows the system to adapt the detection process to the specific characteristics of each image, enhancing the sensitivity and accuracy of kidney stone identification. Additionally, the use of dynamic thresholding reduces the likelihood of misclassification that can occur if a fixed threshold is used across the entire dataset.

3.2 Processing Time for Detection Kidney Stone

The processing times presented in Table 1 reflect the duration required to diagnose kidney stones after selecting the right and left kidney regions. This time includes the entire image processing sequence, from grayscale conversion, kidney area segmentation, binarization, to kidney stone identification. The measurement results indicate that the shortest processing time for kidney stone diagnosis is 1.30 seconds, while the longest recorded time is 1.46 seconds, with an average processing time of approximately 1.32 seconds. This variation in processing time is influenced by the complexity of the image, the size of the kidney area being processed, and the number and size of the detected kidney stones. Interestingly, as shown in Table 1, images without kidney stones tend to have shorter processing times, typically around 1 second. This is likely due to the reduced computational effort required to analyze more homogeneous areas without the presence of dense objects like kidney stones.

In contrast, when the image contains kidney stones, the processing time increases significantly, ranging from 20 seconds to 70 seconds, depending on the size and number of kidney stones detected. Larger or more numerous kidney stones require more time to identify and measure, as they involve a greater number of pixels that must be examined during the segmentation and analysis process. This is demonstrated in the diagnosis of the image from sample data 14 (left kidney area), where the processing time reached 2.21 seconds (see Table 1). This longer processing time can be attributed to the larger number of pixels involved, as shown in Table 2, where sample data 14 has the highest pixel count, totaling 542 pixels, with a kidney stone area of 322.59 mm².

Table 2: Output the pixels count and kidney stone areas.

No.	Code Data	Pixel Count		Kidney Stone Area	
		Right	Left	Right	Left
1	Data 5	-	147	-	140.19
		-	31	-	29.56
2	Data 6	134	-	46.01	-
3	Data 7	34	-	11.67	-
		134	-	46.01	-
4	Data 8	-	117	-	20.44
5	Data 9	118	78	25.93	17.14
		108	-	23.73	-
6	Data 10	60	200	12.15	40.49
7	Data 11	11	-	3.78	-
		57	-	19.57	-
8	Data 12	42	-	40.05	-
		6	-	5.72	-
		57	-	54.36	-
9	Data 13	-	273	-	162.49
		-	23	-	13.69
		-	24	-	14.29
		-	162	-	96.42
10	Data 14	-	542	-	322.59
		-	103	-	61.30
11	Data 15	-	19	-	18.12
		-	11	-	10.49
		-	66	-	62.94
12	Data 16	27	55	9.27	18.88
		47	-	16.14	-
13	Data 17	47	2	44.82	1.91

These differences highlight the importance of optimizing image processing algorithms to ensure high diagnostic accuracy without sacrificing processing efficiency, especially in clinical applications where rapid response times are critical for medical decision-making.

3.3 Correlation between Pixel Count and Kidney Stone Area

The results of the correlation analysis between pixel count and kidney stone area for the right and left kidney regions show significant differences in the strength of the linear relationship, as illustrated in Figure 11.

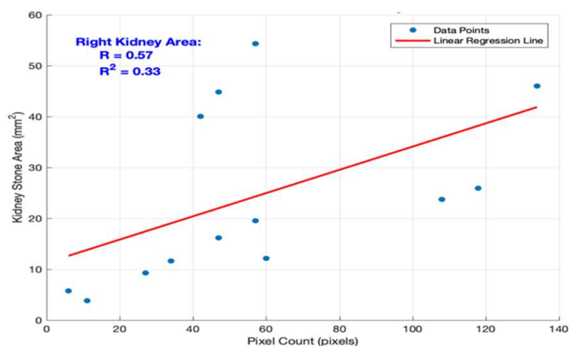

(a) In the right kidney area

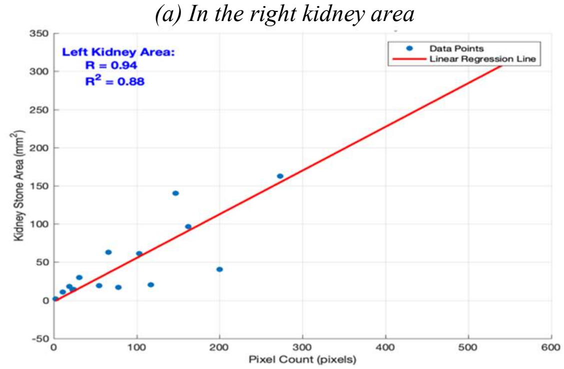

(b) In the left kidney area

Figure 11: Correlation between Pixel Count and Kidney Stone Area.

This variation in resolution during DICOM image capture, as illustrated in Figure 9, further contributes to the observed differences in correlation strength. In the right kidney area, the analysis produced a Correlation Coefficient (R) of 0.57 and a Coefficient of Determination (R^2) of 0.33. This R value indicates a moderate positive relationship between pixel count and kidney stone area, but with a relatively weak overall correlation. The R^2 value of 0.33 suggests that only about 33% of the variation in kidney stone area in the right kidney can be explained by the pixel count, while the remaining 67% is likely influenced by other factors, such as stone shape, distribution, and intensity.

In contrast, for the left kidney area, the analysis yielded a Correlation Coefficient (R) of 0.94 and a Coefficient of Determination (R^2) of 0.88. This indicates a very strong linear relationship between pixel count and kidney stone area, where approximately 88% of the variation in kidney stone area can be explained by the pixel count. This strong correlation suggests that the stone size in the left kidney is more consistently reflected in the pixel count, resulting in a higher overall correlation. This difference may be due to variations in the structure of kidney stones between the right and left kidneys, as well as differences in image quality that can affect the segmentation and detection processes. Additionally, the correlation between pixel count and kidney stone area is also influenced by the resolution of the original CT-Scan images, as shown in Table 1 (column Elliptical Shape Resolution). The kidney regions often have elliptical shapes with different dimensions, resulting in variations in pixel density. This can significantly impact the accuracy of stone size estimation, as larger elliptical areas can contain more pixels, leading to higher area measurements, while smaller elliptical regions may limit the number of detectable pixels.

3.4 Critical Analysis and Comparison with Prior Work

The findings of this study, particularly the average processing time of 1.32 seconds, demonstrate a notable efficiency in kidney stone identification. When compared to the optimized deep learning fusion models [26], which achieve superior accuracy but require substantial computational resources for inference, our method provides a more accessible alternative for immediate clinical screening. Furthermore, while [27] emphasized the importance of image enhancement in CT scans, our study goes a step further establishing a quantifiable correlation between pixel density and physical stone area (mm^2), achieving a strong R-value of 0.94 in the left kidney region.

However, a critical assessment of these results reveals areas of concern that still need attention. The reliance on manual elliptical cropping, while effective in reducing noise, introduces a degree of human subjectivity that could lead to variability in results. Additionally, our findings show that the right kidney correlation (R = 0.57) significantly lower than the left, suggesting that anatomical variations or noise level in specific DICOM slices can impact the consistency of pixel-to-area translation. This highlights an open issue: the need for an automated ROI (Region of Interest) detection to minimize human intervention.

4. CONCLUSION

This study successfully demonstrates the application of image processing techniques for automated kidney stone detection using DICOM medical images. The results indicate that the proposed method can accurately identify kidney stones with varying sizes and shapes, as evidenced by the significant correlation between pixel count and stone area. The right kidney showed a moderate correlation (R = 0.57, R^2 = 0.33), while the left kidney exhibited a much stronger correlation (R = 0.94, R^2 = 0.88), suggesting more consistent relationships in the left kidney area.

Moreover, the processing time varied depending on the presence and size of the kidney stones, with the shortest processing time being 1.30 seconds and the longest 2.21 seconds for larger stones. These findings highlight the importance of efficient algorithm design to handle varying stone sizes and image complexities.

In the authors' opinion, as the field moves toward increasingly complex AI, there is an enduring value in "understandable" image processing techniques that prioritize speed and clinical accessibility over sheer model complexity.

Overall, this approach establishes a reliable framework for kidney stone detection with clear clinical potential for early diagnosis. Future work should focus on integrating adaptive filtering to stabilize thresholding and implementing automated ROI detection to eliminate manual bias. Furthermore, combining this method with machine learning techniques could further enhance both accuracy and processing efficiency.

REFERENCE:

[1] S. Harper and R. Unwin, "Structure and function of the kidney," in *Oxford Textbook of Medicine*, Oxford University Press, 2020. Accessed: Jan. 18, 2025. [Online]. Available: https://academic.oup.com/book/41095/chapter-abstract/351118705?redirectedFrom=fulltext

[2] L. M. A. Barnett and B. S. Cummings, "Nephrotoxicity and Renal Pathophysiology: A Contemporary Perspective," *Toxicological Sciences*, vol. 164, no. 2, pp. 379–390, Aug. 2018, doi: 10.1093/toxsci/kfy159.

[3] F. L. Coe, "Kidney stone disease," *Journal of Clinical Investigation*, vol. 115, no. 10, pp. 2598–2608, Oct. 2005, doi: 10.1172/JCI26662.

[4] D. J. Kok, W. Boellaard, Y. Ridwan, and V. A. Levchenko, "Timelines of the 'free-particle'

ISSN: 1992-8645 www.jatit.org E-ISSN: 1817-3195

and ‘fixed-particle’ models of stone-formation: theoretical and experimental investigations,” *Urolithiasis*, vol. 45, no. 1, pp. 33–41, Feb. 2017, doi: 10.1007/s00240-016-0946-x.

[5] C. D. Scales, A. C. Smith, J. M. Hanley, and C. S. Saigal, “Prevalence of Kidney Stones in the United States,” *European Urology*, vol. 62, no. 1, pp. 160–165, Jul. 2012, doi: 10.1016/j.eururo.2012.03.052.

[6] Z. Wang, Y. Zhang, J. Zhang, Q. Deng, and H. Liang, “Recent advances on the mechanisms of kidney stone formation (Review),” *International Journal of Molecular Medicine*, vol. 48, no. 2, pp. 1–10, Aug. 2021, doi: 10.3892/ijmm.2021.4982.

[7] T. Alelign and B. Petros, “Kidney Stone Disease: An Update on Current Concepts,” *Advances in Urology*, vol. 2018, pp. 1–12, 2018, doi: 10.1155/2018/3068365.

[8] K. Sakhaee, N. M. Maalouf, and B. Sinnott, “Kidney Stones 2012: Pathogenesis, Diagnosis, and Management,” *The Journal of Clinical Endocrinology & Metabolism*, vol. 97, no. 6, pp. 1847–1860, Jun. 2012, doi: 10.1210/jc.2011-3492.

[9] S. A. Howles and R. V. Thakker, “Genetics of kidney stone disease,” *Nat Rev Urol*, vol. 17, no. 7, pp. 407–421, Jul. 2020, doi: 10.1038/s41585-020-0332-x.

[10] J. B. Ziemba *et al.*, “A User-Friendly Application to Automate CT Renal Stone Measurement,” *Journal of Endourology*, vol. 32, no. 8, pp. 685–691, Aug. 2018, doi: 10.1089/end.2018.0326.

[11] Janarthanan. S, Ashok. A, Guruprasad. S. S, Mounesa. P, M. Mohan. M, and Baluprithviraj. K. N, “Investigation of Kidney Stone Detection using Image Processing,” in *2022 International Conference on Edge Computing and Applications (ICECAA)*, Oct. 2022, pp. 946–951. doi: 10.1109/ICECAA55415.2022.9936089.

[12] D. C. Elton, E. B. Turkbey, P. J. Pickhardt, and R. M. Summers, “A deep learning system for automated kidney stone detection and volumetric segmentation on noncontrast CT scans,” *Medical Physics*, vol. 49, no. 4, pp. 2545–2554, 2022, doi: 10.1002/mp.15518.

[13] S. Qadri, “Role of Machine Vision For Identification of Kidney Stones Using Multi Features Analysis,” *Research Journal Of Computer Science And Information Technology*, vol. 5, no. 3, pp. 1–14, Sep. 2021, doi: 10.54692/lgurjcsit.2021.0503212.

[14] P. T. Akkasaligar, S. Biradar, and S. Badiger, “Segmentation of Kidney Stones in Medical Ultrasound Images,” in *Recent Trends in Image Processing and Pattern Recognition*, K. C. Santosh and R. S. Hegadi, Eds., Singapore: Springer, 2019, pp. 200–208. doi: 10.1007/978-981-13-9184-2_18.

[15] D. S. Kim, S. K. Moon, and S. H. Lee, “Histogram of kidney stones on non-contrast computed tomography to predict successful stone dusting during retrograde intrarenal surgery,” *World J Urol*, vol. 39, no. 9, pp. 3563–3569, Sep. 2021, doi: 10.1007/s00345-021-03659-9.

[16] S. Yoshida *et al.*, “Role of volume and attenuation value histogram of urinary stone on noncontrast helical computed tomography as predictor of fragility by extracorporeal shock wave lithotripsy,” *Urology*, vol. 68, no. 1, pp. 33–37, Jul. 2006, doi: 10.1016/j.urology.2006.01.052.

[17] A. Soni and A. Rai, “Kidney Stone Recognition and Extraction using Directional Emboss & SVM from Computed Tomography Images,” in *2020 Third International Conference on Multimedia Processing, Communication & Information Technology (MPCIT)*, Dec. 2020, pp. 57–62. doi: 10.1109/MPCIT51588.2020.9350388.

[18] M. George and A. HB, “Kidney Abnormalities Detection and Classification Using CNN-based Feature Extraction,” in *2022 4th International Conference on Circuits, Control, Communication and Computing (I4C)*, Dec. 2022, pp. 359–362. doi: 10.1109/I4C57141.2022.10057855.

[19] P. Rajan G, P. Sapra, S. S. C. Mary, A. Chauhan, S. A. Parte, and N. Nishant, “Hybrid Convolutional Neural Network and Extreme Learning Machine for Kidney Stone Detection,” in *2023 Second International Conference on Electronics and Renewable Systems (ICEARS)*, Mar. 2023, pp. 936–942. doi: 10.1109/ICEARS56392.2023.10085243.

[20] P. Musa, F. A. Rafi, and M. Lamsani, “A review: Contrast-limited adaptive histogram equalization (CLAHE) methods to help the application of face recognition,” in *3rd International Conference on Informatics and Computing (ICIC)*, IEEE, 2018, pp. 1–6. doi: 10.1109/IAC.2018.8780492.

[21] Neha J. Rao, H. Girish, M.C. Gowrishankar, Shiva Kumar, Nitesh Kumar. "A two-stage deep learning framework for kidney stone detection and clinical severity grading in CT

imaging". Informatics in Medicine Unlocked, Vol. 59. 2025. doi: 10.1016/j.imu.2025.101704.

[23] H. Lusic and M. W. Grinstaff, "X-ray-Computed Tomography Contrast Agents," *Chem. Rev.*, vol. 113, no. 3, pp. 1641–1666, Mar. 2013, doi: 10.1021/cr200358s.

[24] I. Różyło-Kalinowska, "Computed Tomography (CT)," in *Imaging of the Temporomandibular Joint*, I. Rozylo-Kalinowska and K. Orhan, Eds., Cham: Springer International Publishing, 2019, pp. 115–123. doi: 10.1007/978-3-319-99468-0_7.

[25] J. Jan, "X-Ray Computed Tomography," in *Medical Image Processing, Reconstruction and Analysis*, 2nd ed., CRC Press, 2019.

[26] Sohaib Asif, Xiaolong Zheng, Yusen Zhu, "An Optimized Fusion of Deep Learning Models for Kidney Stone Detection from CT Images." Journal of King Saud University - Computer and Information Sciences. Vol. 36 Issue 7, 2024. doi: 10.1016/j.jksuci.2024.102130.

[27]Amruth V, Jeevan B C, Sharath S, R P Pavan Kumar, Shailesh S, "Stone Detection in Kidney with Image Processing: CT Images." International Journal of Creative Research Thoughts (IJCRT), Vol. 12 Issue 5, May 2024. ISSN: 2320-2882.